Solid Freeform Fabrication 2022: Proceedings of the 33rd Annual International Solid Freeform Fabrication Symposium – An Additive Manufacturing Conference
Reviewed Paper

MODELLING FIBER ORIENTATION DURING ADDITIVE MANUFACTURING-COMPRESSION MOLDING PROCESSES

Berin Šeta [1*], Md. Tusher Mollah[1], Vipin Kumar[2], Deepak Kumar Pokkalla[2], Seokpum Kim[2], Ahmed Arabi Hassen[2] and Jon Spangenberg[1]

[1]Department of Civil and Mechanical Engineering, Technical University of Denmark, 2800 Kgs. Lyngby, Denmark
[2]Manufacturing Science Division, Oak Ridge National Laboratory, TN 37932, United States
*Corresponding author: berse@mek.dtu.dk

Abstract

The production of high-performance thermoplastic composites reinforced with short carbon fibers can be achieved by a novel "additive manufacturing-compression molding" technique. An advantage of such a combination is two-fold: controlled fiber orientation in additive manufacturing and less void content by compression molding. In this study, a computational fluid dynamics model has been developed to predict the behavior of printed layers during fiber-reinforced thermoplastic extrusion and subsequent compression molding. The fiber orientation was modelled with the simple quadratic closure model. The interaction between the fibers was included using a rotary diffusion coefficient that becomes significant in concentrated regimes. Finally, the second rank orientation tensor was coupled with the momentum equation as an anisotropic part of the stress term. The effect of different fiber orientation within printed layers was investigated to determine the favorable printing scenarios in the strands that undergo compression molding afterwards. The developed numerical model enables design of high-performance composites with tunable mechanical properties.

Introduction

Additive manufacturing (AM) or 3D printing of polymer composites has been of growing interest in recent years as it enables manufacturing of strong, stiff, and tough parts without the need for multiple processes or special tools [1]. Despite significant advancements demonstrating AM as an excellent tool for prototyping, AM-based manufacturing processes still face some critical challenges. One of the challenges is to eliminate the excessive porosity in printed beads and the subpar bead-to-bead interface that cause poor mechanical properties of 3D printed parts [2, 3]. Nevertheless, AM can remarkably align the fibers in the deposition direction due to the shear stresses developed during the extrusion of the material inside the nozzle. It is well recognized that low porosity and high fiber orientation are essential to achieve excellent mechanical properties for composite parts [1]. Traditionally, extrusion compression molding (ECM) and injection molding (IM) processes are used for the mass production of polymer-based automotive parts with low void contents. In ECM, a plasticizer is used to create a polymer charge (a combination of polymer and fibers) and place it on the mold. The loaded mold then undergoes a compression cycle. As a result, we get fiber-rich or resin-rich areas without control over the fiber alignment during the compression cycle. These non-homogenous areas can create undesirable stress concentration zones in the part. Similarly, with injection molding, we get weak and strong zones within a part because of the different fiber orientations at distinct locations. The location for material injection and the dimensions (especially thickness) of the part determine the fiber orientation of the injection molded parts. The fiber-rich or resin-rich areas in the CM or IM parts leads to overdesign or inefficiency in these traditional composite manufacturing processes. In the end, there is a need for a novel manufacturing process that takes advantage of control over fiber alignment in the AM system and combines with traditional manufacturing processes that produce parts with low porosity levels.

A novel "additive manufacturing – compression molding" (AM-CM) technique was introduced recently to control the fiber orientation (microstructure) while reducing the porosity to produce high-performance fiber-reinforced thermoplastic composite parts [4, 5]. The digital nature of AM systems and high fiber alignment of the deposition process enables local control and tunability of the fiber orientation in each layer and through the thickness of the manufactured parts. The compression molding process produces parts with low porosity levels at rapid processing cycle times. The AM-CM process offers control over various processing parameters and emerges as a game-changing manufacturing technique to produce high-performance composite parts [4]. It allows rapid creation of multi-material parts with tunable mechanical properties via control over the printing toolpath. Consequently, the AM-CM manufacturing technique produces enhanced design freedom with potential cost savings through optimizing materials, intermediates, process flow, cycle times, and integration.

In this paper, a computational fluid dynamics model for the AM-CM process with fiber orientation was developed to predict the behavior of printed layers during fiber-reinforced thermoplastic extrusion and subsequent compression molding. The resultant fiber orientation in the AM-CM parts can be extracted from the numerical model and used to predict the mechanical properties of the composite parts [6]. The paper is organized as follows: Section two presents a general numerical framework with governing equations. Section three describes the modeling of fiber orientation. In the fourth section, the modeling of fiber orientation in an additively manufactured strand and thermoplastic extrusion through a fused deposition modeling process is detailed. In the fifth section, the numerical model for compression molding of AM preforms and the change in fiber orientation within the strand is described. The paper ends with concluding remarks in the sixth section.

General numerical framework

This section describes a numerical model entailing both the additive manufacturing and compression molding processes that result in two steps of the simulation process. While numerical modeling of both techniques is described in the literature [7-13], this is the first report that presents a numerical framework coupling both these techniques together. Both the steps of the simulation are carried out using OpenFOAM, an open-source package, where chimera/overset mesh methodology is used to simulate the movement of the nozzle in the first step, and a compression plate is used in the second step. OpenFOAM was previously used to model the injection molding and fused deposition processes [14-18]. While modeling of injection molding does not require any mesh movement, the fused deposition is modeled using a deformable mesh to simulate substrate movement. In addition, since the thermoplastic polymer is reinforced with fibers, fiber orientation must be coupled with the polymer flow to provide a reasonably accurate result. Previous works on modeling material extrusion additive manufacturing of fiber reinforced thermoplastics considered finite element method (FEM) [19, 20] and smooth-particle hydrodynamics (SPH) [21-23]. In the present work, finite volume method (FVM) is used instead. More specifically, the well-established volume-of-fluid method was used to solve two-phase flow (polymer and air) [24-26]. This approach solves the single momentum equation for both phases, while the interface between those two phases is tracked by the scalar α. Both phases, depending on the value of α, can have different thermophysical and rheological properties.

The continuity and momentum equations can be written as:

$$\nabla . \boldsymbol{u} = 0 \tag{1}$$

$$\rho \left(\frac{\partial \boldsymbol{u}}{\partial t} + \boldsymbol{u} . \nabla \boldsymbol{u} \right) = \rho \boldsymbol{g} + \nabla \sigma \tag{2}$$

where $\boldsymbol{u}$ is the velocity vector, ρ =1250 kg.m^{-3} is the fiber reinforced polymer density, p is the pressure, $\boldsymbol{g}$ is the gravitational acceleration vector with components $(0,0,-g)$, t is the time, and σ the stress-tensor. The latter can be expressed as:

$$\sigma = -p\boldsymbol{I} + 2\mu(\boldsymbol{D} + N_P\boldsymbol{A_{(4)}}\boldsymbol{D}) \quad (3)$$

where $\dot{\boldsymbol{\gamma}} = \sqrt{2\boldsymbol{D} : \boldsymbol{D}}$ is the strain rate magnitude, $\boldsymbol{D} = \left((\nabla \boldsymbol{u}) + (\nabla \boldsymbol{u})^T\right)/2$ is the deformation rate tensor, and μ is the apparent viscosity of the material. The term $N_P\boldsymbol{A_{(4)}}\boldsymbol{D}$ in stress-tensor is contributed by the reinforcing fibers and will be discussed later along with the description of fiber orientation modeling. The rheological behavior of the material is modelled with Carreau-Yasuda shear thinning fluid model [21] and it can be defined as:

$$\mu = \mu_\infty + (\mu_0 - \mu_\infty)(1 + (\tau\dot{\gamma})^a)^{(\frac{n-1}{a})} \quad (4)$$

where μ_∞ is viscosity at the infinite shear rate, μ_0 is viscosity at the zero-shear rate, τ is the relaxation time, n is the power law index, and a is the transition parameter between Newtonian and power law region. Properties of the material are presented in the Table 1 [21].

Table 1: Rheological model parameters

$\boldsymbol{\mu_\infty}$	$\boldsymbol{\mu_0}$	$\boldsymbol{\tau}$	**a**	**n**
10 Pa.s	1450 Pa.s	0.0045 s	1	0.09

Finally, the phase fraction scalar α is transported by:

$$\frac{\partial \alpha}{\partial t} + \nabla(\alpha \boldsymbol{u}) = 0 \quad (5)$$

The thermophysical properties on the interface, where value α is between 0 and 1, are interpolated with the mixture rule. This applies to all thermophysical properties, including density and viscosity which are the most relevant in this case. The equation describing the density on the interface is given in Eq. (6),

$$\rho = \rho_P\alpha + \rho_A(1 - \alpha) \quad (6)$$

where ρ_P is the density of the polymer and ρ_A is the density of air.

It is important to highlight that the phases are modeled as incompressible fluids as can be seen from the momentum and continuity equation. Assuming phases to be incompressible for the FDM process is perfectly valid whereas in the case of squeezing/compression, this assumption is valid until some level of compression only. Hence, the current study does not consider high level of squeezing. The problem is formulated as isothermal, which means that viscosity does not depend on temperature. The boundary conditions for the velocity include prescribed extrusion speed U in the inlet of the nozzle and a no-slip boundary condition on the walls of the nozzle and the substrate. For the imaginary walls surrounding the substrate and the nozzle bounding the numerical mesh, pressure must be specified. It imposes zero-gradient for the outflow while the velocity for the inflow is obtained from the internal cell. When combined with the boundary condition for the phase fraction α at the same walls, this allows material to escape from the domain without being constrained, if the flow conditions for such a scenario arise. The phase fraction α has a value 1 at the inlet patch in the nozzle. The walls of the nozzle and substrate are prescribed with zero-gradient boundary condition. The fiber's orientation tensor **A** is prescribed with a perfectly random orientation at the inlet in the nozzle, while zero gradient is prescribed for all the other boundary conditions.

Modeling fiber orientation

Composite material flow can be simulated using different approaches [27-29]. Two main categories are represented as microscopic and macroscopic models. Microscopic models would require using either SPH or discrete element method (DEM), or *simply* tracking each fiber in the polymer matrix using a Lagrangian approach. However, as the number of fibers inside the material can be very high, this tends to be very computationally

expensive. On the other hand, macroscopic models offer an alternative to the microscopic models based on the Jeffery´s formulation of the motion of a single particle within the fluid flow [30]. The basic model is extended by Folgar and Tucker, which included fiber-fiber interaction under the assumption of incompressibility of the fluid and negligible Brownian motion [31]. Finally, a transport equation fiber orientation tensor **A** is proposed by Advani and Tucker [32], with different closure approximations [33]. This model is included in some of the commercially available software such as Moldflow and Moldex 3D. However, such a model does not exist in OpenFOAM requiring it to be implemented. This model was first implemented by Kerstin [34] for single-phase fluid flows and then extended to both incompressible and compressible reactive multiphase flows for injection molding applications [14 – 17, 35]. However, those multiphase solvers which model the fiber orientation tensor transport equation do not allow the use of overset/chimera grid, which is necessary for modeling the AM-CM process. The transport equation of second rank orientation tensor **A** can be written as:

$$\frac{\partial \boldsymbol{A}}{\partial t} + (\boldsymbol{u} \cdot \boldsymbol{\nabla})\boldsymbol{A} = -(\boldsymbol{W} \cdot \boldsymbol{A} - \boldsymbol{A} \cdot \boldsymbol{W}) + \lambda_F\left(\boldsymbol{D} \cdot \boldsymbol{A} + \boldsymbol{A} \cdot \boldsymbol{D} - 2\boldsymbol{D} : \boldsymbol{A}_{(4)}\right) + 2D_r(\boldsymbol{I} - 3\boldsymbol{A}) \qquad (7)$$

where λ_F is the shape factor, $\boldsymbol{W}$ is the vorticity tensor, $\boldsymbol{A}_{(4)}$ is the fourth rank orientation tensor, D_r is the rotary diffusion coefficient that is used to model the fiber-fiber interactions. A closure approximation is required for the term $\boldsymbol{A}_{(4)}$ to solve the equation above. Among various closure approximations explored in the literature [33, 36, 37], a simple quadratic closure approximation is used here. Hence, $\boldsymbol{A}_{(4)}$ is the dyadic product of the second rank order tensor $\boldsymbol{A}$ by itself ($\boldsymbol{A}_{(4)} = \boldsymbol{A} \otimes \boldsymbol{A}$). It is evident from Eq. (7) that both the strain-rate deformation tensor **D** and vorticity tensor **W** will influence the orientation tensor **A**. However, the problem is coupled back in the momentum equation through the stress term, where $N_P\boldsymbol{A}_{(4)}\boldsymbol{D}$ term is present. As it can be seen, the orientation tensor will influence the rheology of the composite material, multiplied by the Np factor, which represents the anisotropy level. The Np factor is modeled in various way [38, 39], but in general it depends on the volume fraction of the fibers and the aspect ratio (length and radius). The rotary diffusion coefficient is defined as $D_r = C\dot{\gamma}$, where the coefficient C is the interaction coefficient. The coefficient C is a function of the volume fraction and the aspect ratio of the fibers. For modeling the fibers, the aspect ratio of the fibers, volume fraction, and the initial orientation tensor **A** are necessary. Two extremes of the initial orientation tensor **A** can be written as,

$$\boldsymbol{A} = \begin{pmatrix} 1 & 0 & 0 \\ 0 & 0 & 0 \\ 0 & 0 & 0 \end{pmatrix} \text{ and } \boldsymbol{A} = \begin{pmatrix} \frac{1}{3} & 0 & 0 \\ 0 & \frac{1}{3} & 0 \\ 0 & 0 & \frac{1}{3} \end{pmatrix} \qquad (8)$$

where the first one is representing the orientation completely aligned with the x-axis, while the second one represents a perfectly random isotropic orientation. Notice that the trace of the tensor must be 1. Results should be interpreted as the probability of the orientation in certain direction, where 0.9 for example, would mean that there is a 90% chance or 90% of fibers are oriented in that direction.

Fused deposition modelling

The first stage represents modeling of FDM. This includes both the flow inside the nozzle and during the deposition onto the substrate. The simulation setup, with highlighted substrate, nozzle and boundary wall patches is illustrated in Fig. 1.

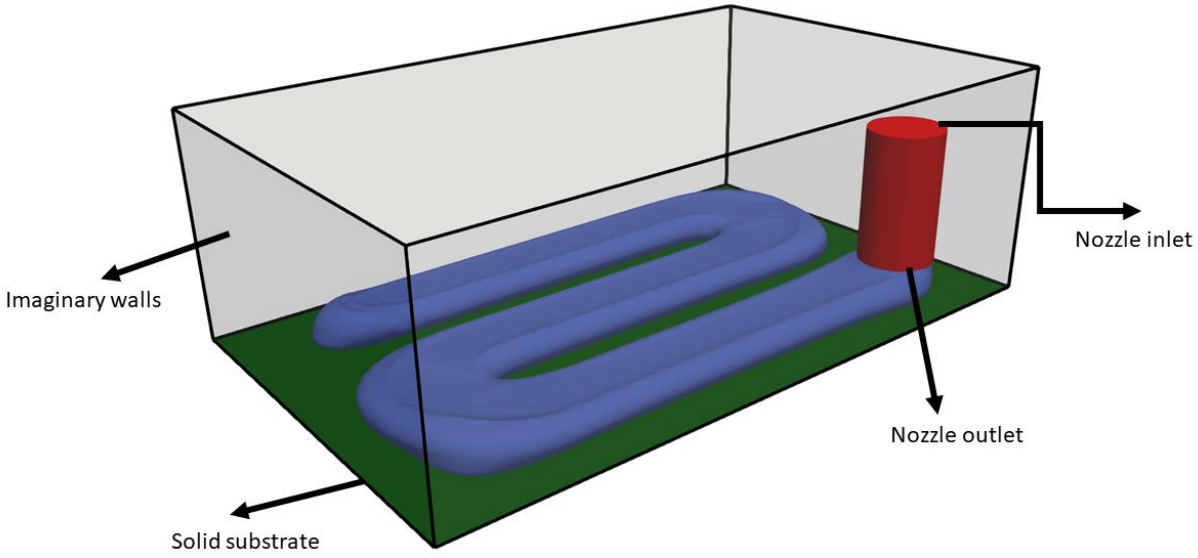

Figure 1: Sketch of fused deposition modeling in OpenFOAM

The flow is initiated from the empty nozzle with composite material that carries on completely randomly oriented fibers as described above. Process parameters and fiber properties are summarized in Table 2.

Table 2: Processing and fiber parameters

U	V	h	D	L	ϕ	Ar
30 mm/s	30 mm/s	12.5 mm	25 mm	75 mm	10%	10

As the flow goes through the nozzle, fibers tend to orientate along the nozzle length, especially in the regions close to the walls. In the central core region, fibers are mostly oriented in a random manner as the material in this core region is unyielded. The orientation of fibers inside the nozzle as well as the profile along the mid cross-section of the nozzle can be seen in Figs. 2 and 3. At a short distance out from the entry of the nozzle (say, 5 mm), the fibers are strongly aligned in the vertical or extrusion direction due to high shear flow. As we move away from the entry of the nozzle, fibers tend to be more aligned in the flow direction (refer transformation from red curve to blue curve in Fig. 3). The difference in fiber orientation decreases as we move away from the entry of the nozzle, as depicted in Fig. 3. The difference is in the central region where fibers are not highly aligned while the orientation of fibers in regions close to the wall does not differ much. This is evident by comparing the cases corresponding to L = 55 mm and L = 30 mm. Using a longer nozzle would not cause further alignment of the fibers in the vertical direction.

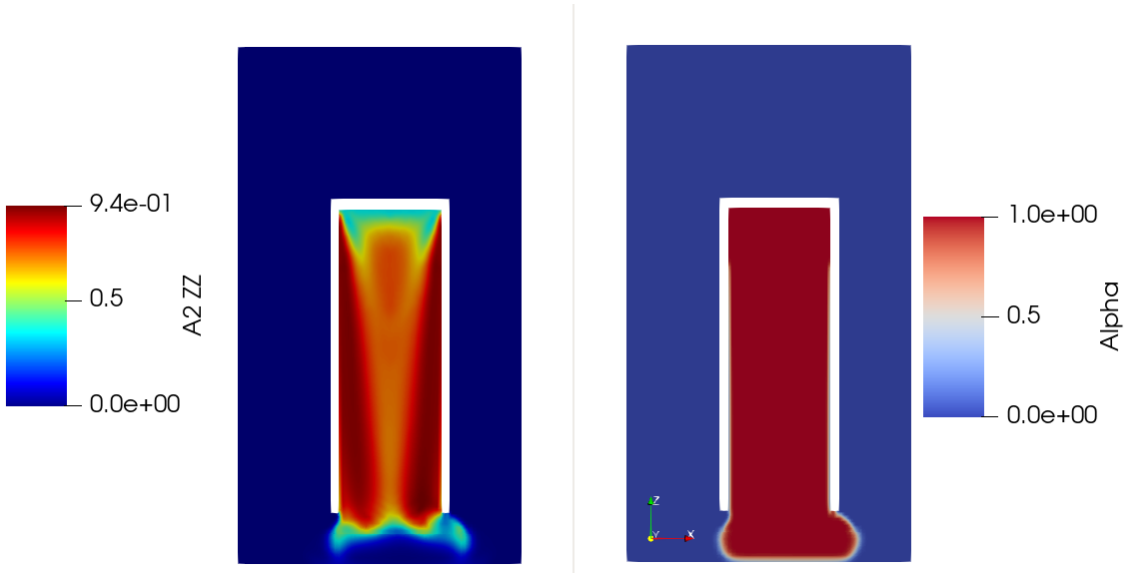

Figure 2: The tensor component that describes orientation of fiber in vertical (z-axis) direction on the left. On the right, α phase fraction plotted, where red color represents the printing strand.

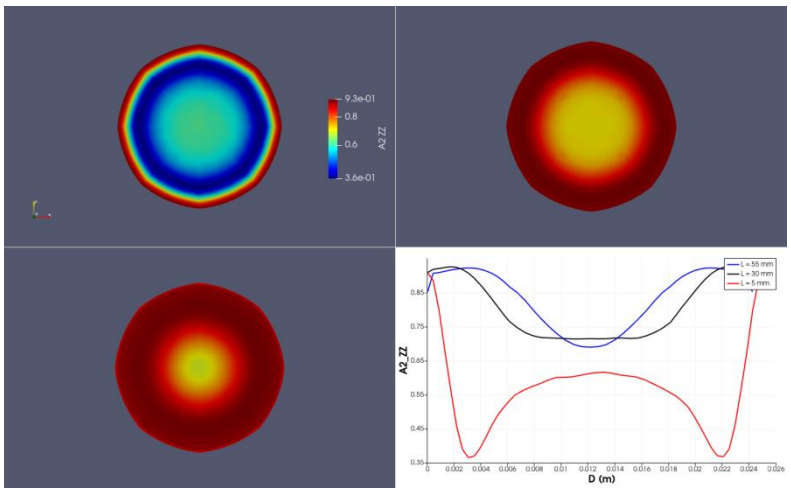

Figure 3: A2_ZZ tensor component on different cross sections in the nozzle. The upper left, right, and bottom left insert figures represent cross-sections at 5 mm, 30 mm, 55 mm below the nozzle entry. The bottom right insert represents value of A2_ZZ component, along the midline plotted for these different cross-sections.

Compared to the existing literature, the present numerical setup offers the capability to examine 3D effects of fiber flow on orientation of fibers and vice versa. The experimental investigation revealed that the orientation of the fibers along the strand is not uniform [40]. Kumar et al. concluded that the AM process yielded panels with 75% of fibers orientated in 0-20 angle for a given set of printing parameters. After compression, the fiber orientation increased to ~82% [4]. A significant side-flow in the third direction (y-axis in Fig. 2), can cause fiber alignment in that direction, and this effect can be seen only via 3D simulations. This effect has been reported and experimentally proven by Quintana et al. [40], where the authors concluded that the fiber orientation was significantly higher in the y-direction as compared to vertical z-direction.

In Fig. 4, probability of fiber orientation along the x-axis (printing direction) and the y-axis (axis representing the strand side flow) across the cross section are depicted. From these cross-sections, two zones can be readily distinguished. First, the skin zone corresponding to the outer part of the strand contains fibers oriented highly in the printing direction. In the core zone formed by the inner part of the strand, the probability for fiber

orientation along y-direction is significant, especially at the bottom of the central core region. This effect is often overlooked by planar simulations. Using the parameters in Table 2, a 67% of fibers in the skin region were found to be oriented in the printing direction (0 – 20 degree), agreeing well with the experimental results from Kumar et al. (75%) [4]. Note that while the h/D ratio is same in both the studies, U/V ratio is different and thus, explains the small discrepancy between the numerical and experimental results. The U/V ratio does affect the orientation of fibers [21]. The maximum probability for fiber orientation from the numerical simulations in skin region is 95% while it 66% in the core region. Small narrow blue regions at the edges of the strand (bottom right insert of Fig. 4) arise in the numerical simulations as the α function (phase fraction) does not have a sharp interface, but rather a diffusive one. The orientation of the fibers is solved in such a way that the magnitude of the **A** tensor is scaled by the α value to prevent numerical escape of the fibers from the material into the air. For that reason, in the zones where α tends to go 0, but it is still >0, the fibers are less oriented.

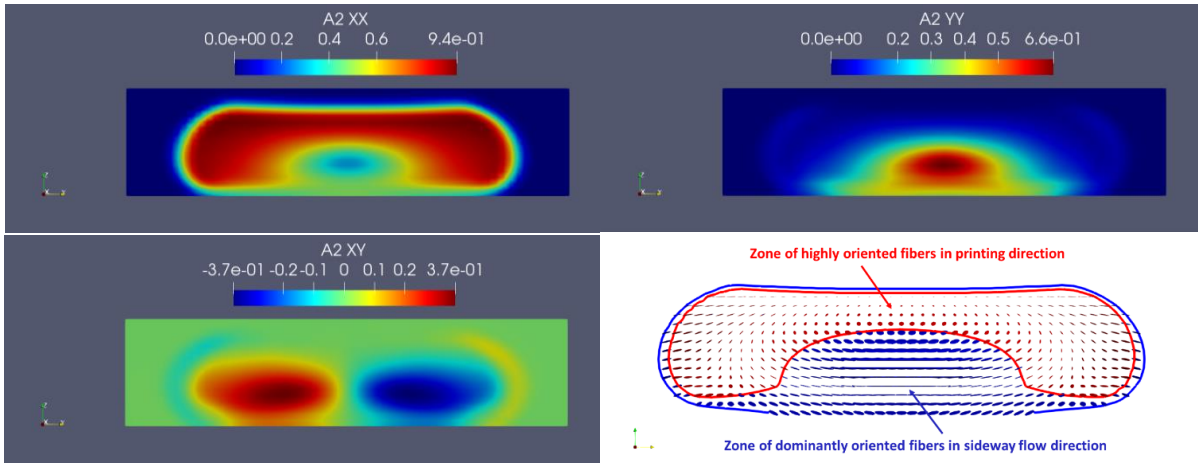

Figure 4: Top left and right inserts represent orientation of the fibers in x-(printing) and y-directions (sideway flow direction). Bottom left insert represent orientation in the x-y direction, while the bottom right insert represents two zones that are delineated depending on dominant orientation of fibers.

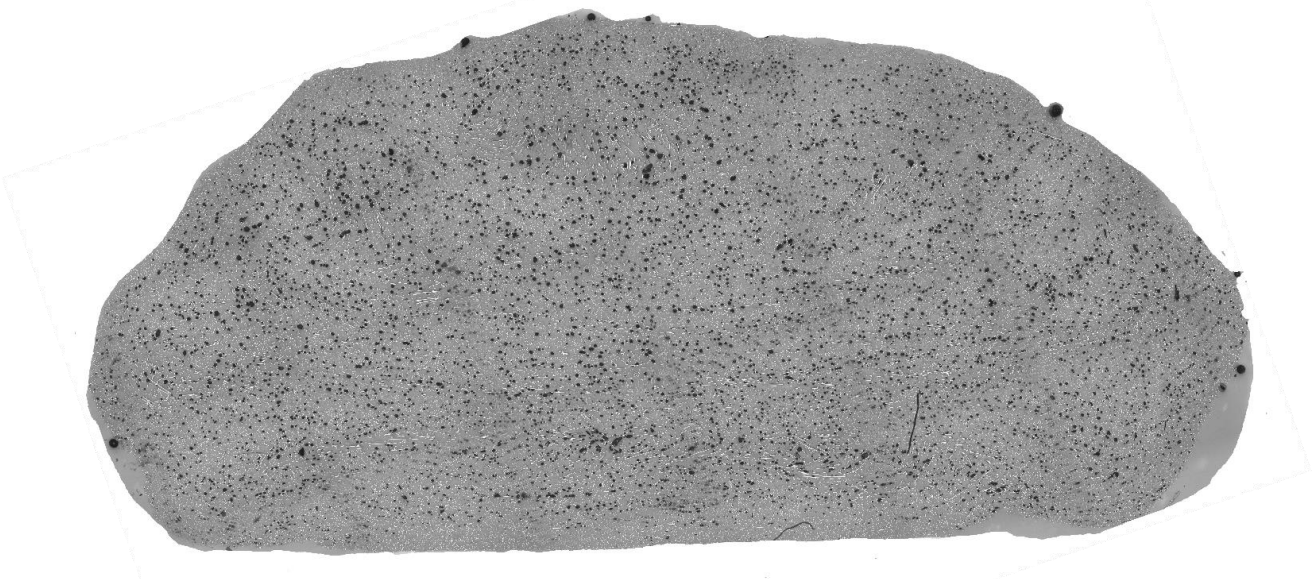

Figure 5. Experimental cross section of the fiber reinforced strand

To prove the existence of the core/skin region, preliminary experimental runs have been done, as shown in Fig. 5. It is possible to see from Fig. 5 that a significant number of fibers are oriented in the horizontal direction, especially in the central zone closer to the bottom of the strand. On the other hand, close to the edges of the strand,

only white dots are visible. This means that fibers in those zones are oriented perpendicular to the strand plane presented in Fig. 5. These experimental finding qualitatively agree with the numerical ones; however more precise and detailed comparison must be done. Note that the fibers in Fig. 5 are represented as thin white lines/dots, while black dots correspond to pores.

It is possible to relate tensor field **A** in the cross section at the end of the nozzle with the cross section of the strand. In both cases, the central region is less oriented in the main-flow direction (deposition/extrusion direction), but it is elongated and shifted to the bottom in the case of the strand. This is a direct consequence of the sideways flow, which can be partially suppressed by a different choice of U/V or h/D ratios. Additionally, an important difference between the fiber orientation in those two core regions is found. In the cross section of the nozzle, the core region is randomly oriented, while in the cross section of the strand, fiber orientation in z-direction is almost non-existent. This feature will point out the fact that vertically oriented fibers in the strand are easily reoriented during sideways flow, which also explains why the core region not only expanded from the nozzle, but also its peak values (A2 YY component) became higher. The initial fiber orientation of these additively manufactured strands plays a significant role in modeling the reorientation of fibers in the subsequent compression molding process and thus the fiber orientations in the AM-CM parts produced.

Compression molding

The second part of the process represents compression molding. In general, when preforms exhibit random orientation of fibers it is hard to estimate and control the final orientation of the fibers after compression. It is possible to see from Kumar et al. that by extrusion compression molding (ECM) only 7% fibers were highly oriented in a given direction [4]. For that reason, the effect of squeezing on the orientation of fibers in the additively manufactured strands is examined here. To begin with, these strands have different fiber orientations corresponding to those from the AM process or initialized manually, emphasizing the importance of the initial fiber's orientation on the final orientation tensor values. The strands obtained by FDM are mapped onto the new numerical mesh prepared for CM, where these strands represent initial condition in the case of CM.

The numerical model used the same set of the equations as the first part representing the AM process; again, using chimera/overset methodology. However, instead of prescribing a velocity to the nozzle as done in the AM part, the velocity is prescribed to the compression press here. Note that the velocity of the press will not affect the way strand is deformed, at least for the two velocities (30 and 60 mm/s) considered here. The compression molding process is illustrated in the Fig. 6. The left top insert shows the non-compressed strand while the top right insert represents the strand undergoing compression. The overset mesh is depicted in the bottom insert of Fig. 6. The blue cells correspond to the ones calculated directly on both the background and overset meshes, while the red ones are blocked, and they represent the compression press. Blocked cells means that no solution is calculated among these cells, and, in this case, they represent a solid body. The green color cells (around red ones) represent the edges of the overset mesh, where the overset boundary condition is applied. In those cells, the solution is interpolated between the overset and the background mesh. This interpolation is the only source of numerically introduced errors because of using the overset mesh. However, the numerical errors could be minimized using different techniques such as using similar size of cells in both the meshes.

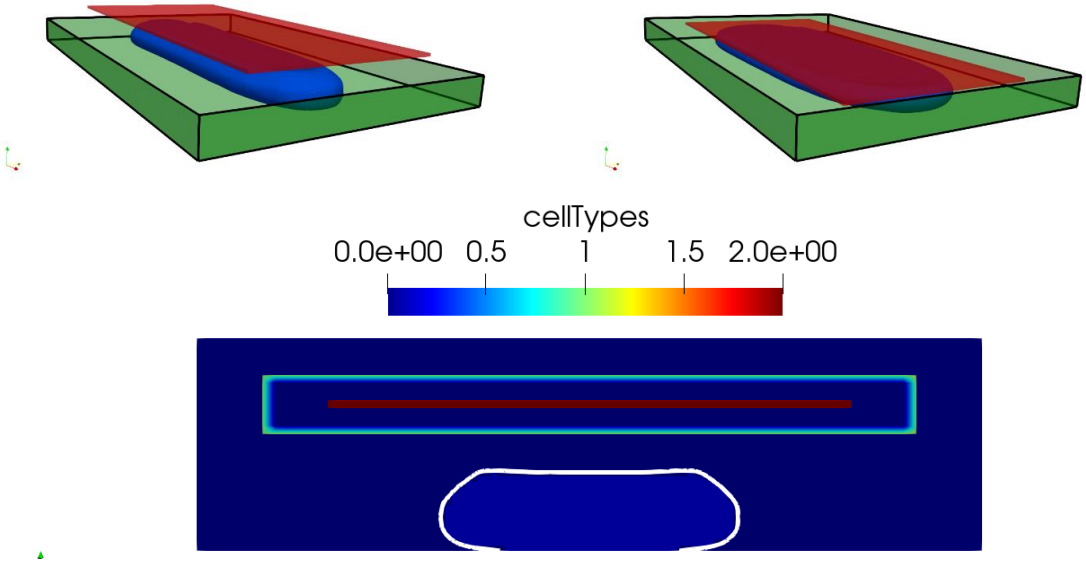

Figure 6: Top left and right inserts represent previously deposited strand and the strand undergoing compression molding. Bottom insert represents identity differentiation between directly calculated cells, blocked cells, and interpolated cells with the use of overset mesh methodology.

The strand appearance and the fiber orientation within the strand are presented in the Fig. 7, for different levels of compression. In the top insert, the strand is not squeezed, in the middle part the strand is squeezed by 3 mm, while in the bottom insert, the strand is squeezed by 6 mm. This illustrates the expansion of the core region with fibers generally oriented along the y-axis (horizontal in this plane). However, the skin region with highly oriented fibers remains unaffected. These results agree well with the experimental observations by Kumar [4], where orientation of fibers along deposition or printing direction became even higher after compression. The maximum values of A2 XX component along the middle slide of the strand get smaller while the compression level is increasing. On the other hand, the maximum values of A2 YY component are getting higher as the main flow direction during the compression step is along the y axis. Not much re-orientation of fibers aligned in the x-direction is observed. As the core region expands under compression, the orientation of fibers in the x-direction (0-20 degree) drops to 43% with 3 mm squeezing and 15% with 6 mm squeezing. This is different from experiments and occurs because of simulating a single strand as compared to experiments involving multiple strands printed next to each other. The side flow during compression is unconstrainted in this study allowing much higher orientation of the fibers in y-direction.

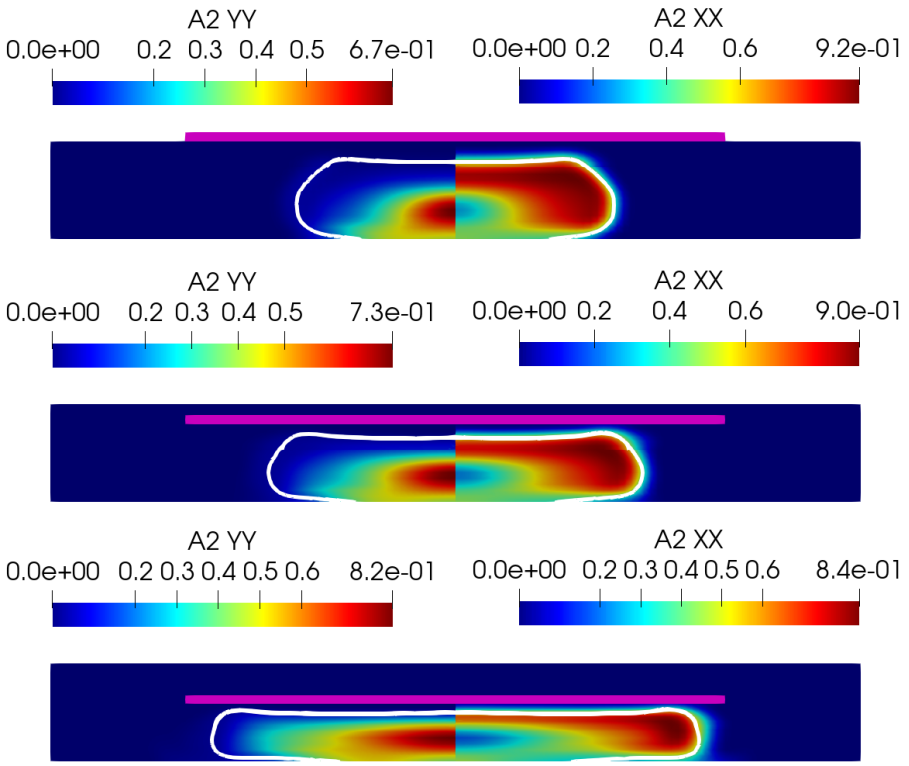

Figure 7: Fiber orientation in x and y direction during compression stage. Top part – uncompressed, middle part – 3 mm compressed, bottom part – 6 mm compressed.

Furthermore, different fiber orientations were considered prior to compression to study the effect of initial fiber orientation obtained from the AM process. In addition to the fiber orientation obtained from the deposition flow simulation, three more cases were considered: perfectly random orientation (0.3333 each diagonal component of A2 tensor), completely aligned in deposition direction (perpendicular to the cross-section plane on Fig. 7) and completely aligned in vertical z-direction (Fig. 7). The resulting A2 YY tensor component for these three cases are illustrated in Fig. 8. Interestingly, the final patterns are not the same neither in terms of shape nor absolute values. While the absolute values are expected to be different due to different initial conditions, fiber re-orientation occurred differently and because of different input parameters. The case with values 0.3333 on main diagonal of the tensor had similar appearance as the one with the completely aligned fibers in x-direction (top and middle part of Fig. 8). The difference between those two was that the skin of the strand is very thin (blue zones on the very edges from the sides) in the case of random orientation while in the case of orientation in x-direction, the skin was thicker. This confirms that the fiber oriented along the printing direction are hard to re-orient while most of the randomly oriented fibers re-orient easily. In contrast, when fibers are aligned in z-direction (vertical axis in this projection), the fibers have the highest degree of the orientation caused due to the side flow which is perpendicular to the length of the fiber. Moreover, the bottom insert in Fig. 8 shows as different pattern. The skin on the sides almost vanishes and the maximum value of the orientation tensor component in the y-direction is very high (0.91). This is a big change especially considering that initially no fibers were oriented in the y-direction. The core part of the strand remains oriented in the z-direction as no flow occurs in the very central part of the strand due to symmetry and hence no re-orientation takes place.

Hence, the computational fluid dynamics model developed in this study for AM-CM process predicts the behavior of additively manufactured and compression molded fiber-reinforced thermoplastic composites. The mechanical properties of the composite parts are highly dependent on the fiber orientation and thus can be predicted by extracting the fiber orientation of AM-CM parts from the numerical model [6, 41]. The obtained engineering

constants can be used for modeling and simulation of the composite parts with a given geometry for various applications using FEM [6, 42].

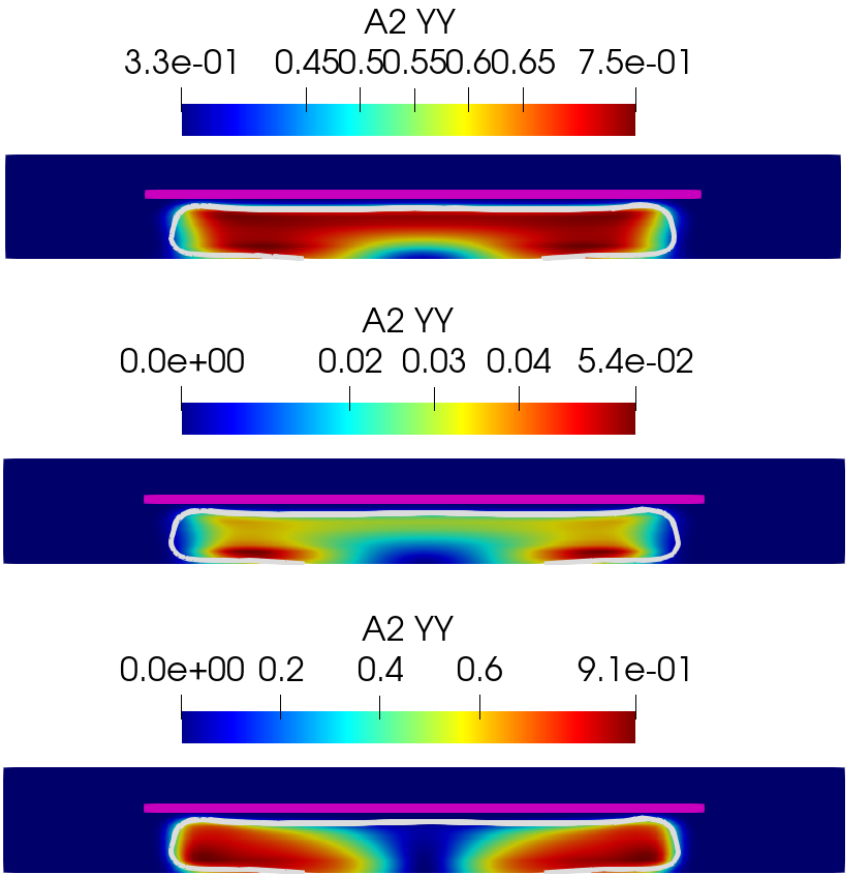

Figure 8: A2 YY component of orientation tensor for three different initial cases of the fiber orientation in the strand. The top part of the figure represents compressed strand with the initially perfectly random fiber orientation. The middle part of the figure represents compressed strand with the initially completely aligned fiber in printing direction (going into cross-section). The bottom part of the figure represents compressed strand with the initial completely aligned fiber in vertical z-direction.

Conclusion

A numerical model integrating both the fiber-reinforced fused deposition modeling and compressive molding process is presented for the first time in this work. The fiber orientation during both these processes was modeled and AM-CM inter coupling is briefly discussed. The numerical simulations involved solving a fully coupled model, where the orientation of fibers is dependent on the fluid flow and stresses in the fluid are affected by the fiber orientation within the strand. The numerical model is unique in terms of its implementation using overset mesh: the model is not restricted to the 2D planar flow, and the nozzle can move freely in any direction. Moreover, an unorthodox approach to compressive molding simulations is presented, where the transient process of squeezing is highlighted and not the final shape of the part. The strands obtained by the FDM are identified with two different regions: skin with highly aligned fibers in the printing direction and core region where fibers are partially oriented in the direction of side flow. Up to now, simulations revealed existence of the core region where fibers are not aligned in the printing direction. But since those simulations were 2D, the shape of the core was not known. These findings regarding existence of core and skin region are reinforced by experimental

findings. Afterwards, the printed strands from FDM part are mapped onto new mesh, where the compression molding is initialized. Subsequent squeezing of strands leads to expansion of the core part, while the skin region remains unaffected. However, once initial condition of fiber orientation inside strand is changed, the pattern of orientation tensor took a different form. Hence, initial fiber orientation within the strand has a high impact on the orientation inside the final compressed strand. This allows control over fiber orientation within strands by varying AM processing parameters and subsequently combining with squeezing through compression molding process to produce high performance fiber-reinforced thermoplastic composites with tunable mechanical properties.

Acknowledgments

The authors BŠ and JS would like to acknowledge the support of the Innovation Fund Denmark (Grant no. 0223-00084B). The research is in part supported by the US Department of Energy (DOE), Office of Energy Efficiency and Renewable Energy, Advanced Manufacturing Office, under contract DE-AC05-00OR22725 with UT-Battelle LLC.

References

[1] Van de Werken, N., Tekinalp, H., Khanbolouki, P., Ozcan, S., Williams, A. and Tehrani, M., 2020. Additively manufactured carbon fiber-reinforced composites: State of the art and perspective. Additive Manufacturing, 31, p.100962.

[2] Tekinalp, H.L., Kunc, V., Velez-Garcia, G.M., Duty, C.E., Love, L.J., Naskar, A.K., Blue, C.A. and Ozcan, S., 2014. Highly oriented carbon fiber–polymer composites via additive manufacturing. Composites Science and Technology, 105, pp.144-150.

[3] Duty, C., Failla, J., Kim, S., Smith, T., Lindahl, J. and Kunc, V., 2019. Z-Pinning approach for 3D printing mechanically isotropic materials. Additive Manufacturing, 27, pp.175-184.

[4] Kumar V, Alwekar SP, Kunc V, Cakmak E, Kishore V, Smith T, Lindahl J, Vaidya U, Blue C, Theodore M, Kim S. High-performance molded composites using additively manufactured preforms with controlled fiber and pore morphology. Additive Manufacturing. 2021;37:101733.

[5] NLN V, Nielson C, Yeole P, Spencer R, Cramer C, Badesha AS, Nuttall D, Vaidya U, Kunc V. Large-scale continuous carbon/glass fiber additive-compression molded composites. Oak Ridge National Lab.(ORNL), Oak Ridge, TN (United States); 2021.

[6] Pokkalla, D.K., Kumar, V., Jo, E., Hassen, A.A., Cakmak, E., Alwekar, S., Kunc, V., Vaidya, U., Baid, H.K. and Kim, S., 2022, April. Anisotropic mechanical properties of polymer composites from a hybrid additive manufacturing-compression molding process using x-ray computer tomography. In Nondestructive Characterization and Monitoring of Advanced Materials, Aerospace, Civil Infrastructure, and Transportation XVI (Vol. 12047, pp. 319-328). SPIE.

[7] Mollah MT, Comminal R, Serdeczny MP, Pedersen DB, Spangenberg J. Stability and deformations of deposited layers in material extrusion additive manufacturing. Additive Manufacturing. 2021; 46: 102193.

[8] Comminal R, Serdeczny MP, Pedersen DB, Spangenberg J. Numerical modeling of the strand deposition flow in extrusion-based additive manufacturing. Additive Manufacturing. 2018;20:68-76.

[9] Comminal R, Hattel JH, Spangenberg J. Numerical simulations of planar extrusion and fused filament fabrication of non-Newtonian fluids. Annu. Trans. Nord. Rheol. Soc.;25:263-70.

[10] Serdeczny MP, Comminal R, Pedersen DB, Spangenberg J. Experimental validation of a numerical model for the strand shape in material extrusion additive manufacturing. Additive Manufacturing. 2018;24:145-53.

[11] Serdeczny MP, Comminal R, Pederson DB, Spangenberg J. Numerical prediction of the porosity of parts fabricated with fused deposition modeling. In 2018 International Solid Freeform Fabrication Symposium 2018. University of Texas at Austin.

[12] Comminal R, Silva WR, Andersen TJ, Stang H, Spangenberg J. Influence of processing parameters on the layer geometry in 3D concrete printing: experiments and modelling. In RILEM international Conference on Concrete and Digital Fabrication 2020(pp. 852-862). Springer, Cham.

[13] Park CH, Lee WI, Yoo YE, Kim EG. A study on fiber orientation in the compression molding of fiber reinforced polymer composite material. Journal of Materials Processing Technology. 2001;111(1-3):233-9.

[14] Krebelj K, Krebelj A, Halilovič M, Mole N. Modeling Injection Molding of High-Density Polyethylene with Crystallization in Open-Source Software. Polymers. 2020;13(1):138.
[15] Pedro J, Ramôa B, Nóbrega JM, Fernandes C. Verification and validation of openInjMoldSim, an open-source solver to model the filling stage of thermoplastic injection molding. Fluids. 2020;5(2):84.
[16] Ospald F. Numerical simulation of injection molding using OpenFOAM. PAMM. 2014;14(1):673-4.
[17] Fontaínhas AM. Injection moulding simulation using OpenFOAM®, 2019; (Doctoral dissertation, Universidade do Minho (Portugal)).
[18] Liu J, Anderson KL, Sridhar N. Direct simulation of polymer fused deposition modeling (fdm)—an implementation of the multi-phase viscoelastic solver in OpenFOAM. International Journal of Computational Methods. 2020;17(01):1844002.
[19] Heller BP, Smith DE, Jack DA. Planar deposition flow modeling of fiber filled composites in large area additive manufacturing. Additive Manufacturing. 2019;25:227-38.
[20] Wang Z, Smith DE. Finite element modelling of fully-coupled flow/fiber-orientation effects in polymer composite deposition additive manufacturing nozzle-extrudate flow. Composites Part B: Engineering. 2021;219:108811.
[21] Bertevas E, Férec J, Khoo BC, Ausias G, Phan-Thien N. Smoothed particle hydrodynamics (SPH) modeling of fiber orientation in a 3D printing process. Physics of Fluids. 2018;30(10):103103.
[22] Ouyang Z, Bertevas E, Parc L, Khoo BC, Phan-Thien N, Férec J, Ausias G. A smoothed particle hydrodynamics simulation of fiber-filled composites in a non-isothermal three-dimensional printing process. Physics of Fluids. 2019;31(12):123102.
[23] Ouyang Z, Bertevas E, Wang D, Khoo BC, Férec J, Ausias G, Phan-Thien N. A smoothed particle hydrodynamics study of a non-isothermal and thermally anisotropic fused deposition modeling process for a fiber-filled composite. Physics of Fluids. 2020;32(5):053106.
[24] Comminal R, Spangenberg J, Hattel JH. Cellwise conservative unsplit advection for the volume of fluid method. Journal of computational physics. 2015;283:582-608.
[25] Comminal R, Spangenberg J. Three-dimensional cellwise conservative unsplit geometric VOF schemes. Journal of Computational Physics. 2021;442:110479.
[26] Hirt CW, Nichols BD. Volume of fluid (VOF) method for the dynamics of free boundaries. Journal of computational physics. 1981;39(1):201-25.
[27] Sandberg M, Yuksel O, Baran I, Spangenberg J, Hattel JH. Steady-state modelling and analysis of process-induced stress and deformation in thermoset pultrusion processes. Composites Part B: Engineering. 2021;216:108812.
[28] Sandberg M, Hattel JH, Spangenberg J. Numerical modelling and optimisation of fibre wet-out in resin-injection pultrusion processes. In European Conference on Composite Materials (ECCM18 conference proceedings, Athens, Greece, 2018) 2018.
[29] Sandberg M, Yuksel O, Baran I, Hattel JH, Spangenberg J. Numerical and experimental analysis of resin-flow, heat-transfer, and cure in a resin-injection pultrusion process. Composites Part A: Applied Science and Manufacturing. 2021;143:106231.
[30] Jeffery GB. The motion of ellipsoidal particles immersed in a viscous fluid. Proceedings of the Royal Society of London. Series A, Containing papers of a mathematical and physical character. 1922;102(715):161-79.
[31] Folgar F, Tucker III CL. Orientation behavior of fibers in concentrated suspensions. Journal of reinforced plastics and composites. 1984;3(2):98-119.
[32] Advani SG, Tucker III CL. The use of tensors to describe and predict fiber orientation in short fiber composites. Journal of rheology. 1987;31(8):751-84.
[33] Advani SG, Tucker III CL. Closure approximations for three-dimensional structure tensors. Journal of Rheology. 1990;34(3):367-86.
[34] Heinen, K. Mikrostrukturelle Orientierungszustände Strömender Polymerlösungen und Fasersupensionen; Universität Dortmund: Dortmund, Germany, 2007
[35] Wittemann F, Maertens R, Bernath A, Hohberg M, Kärger L, Henning F. Simulation of reinforced reactive injection molding with the finite volume method. Journal of Composites Science. 2018;2(1):5.
[36] Férec J, Bertevas E, Ausias G, Phan-Thien N. Macroscopic modeling of the evolution of fiber orientation during flow. In Flow-induced alignment in composite materials 2022;(pp. 77-121). Woodhead Publishing.

[37] Kugler SK, Kech A, Cruz C, Osswald T. Fiber orientation predictions—a review of existing models. Journal of Composites Science. 2020;4(2):69.
[38] Dinh SM, Armstrong RC. A rheological equation of state for semiconcentrated fiber suspensions. Journal of Rheology. 1984;28(3):207-27.
[39] Phan-Thien N, Graham AL. A new constitutive model for fibre suspensions: flow past a sphere. Rheologica acta. 1991;30(1):44-57.
[40] Colón Quintana JL, Slattery L, Pinkham J, Keaton J, Lopez-Anido RA, Sharp K. Effects of Fiber Orientation on the Coefficient of Thermal Expansion of Fiber-Filled Polymer Systems in Large Format Polymer Extrusion-Based Additive Manufacturing. Materials. 2022;15(8):2764.
[41] Sharma, I., Kumar, P.D. and Maiti, P.R., 2015. The effect of fiber orientation and laminate layup on fiber-reinforced polymer composite. *IUP Journal of Structural Engineering*, *8*(1), p.49.
[42] Kumar, P.D., Sharma, I. and Maiti, P.R., 2014. Parametric Study of a Simply Supported Composite Plate Using Finite Element Method. *i-Manager's Journal on Civil Engineering*, *4*(4), p.26.